Proc. Natl. Sci. Counc. ROC(A)
Vol. 20, No. 2, 1996. pp. 158-165

Thermophysical Calculation of X-Ray Mask for Quarter-Micron Lithography

DZ-CHI LI*, JENG-TZONG CHEN**, CHIANG-WOEI CHYUAN*** AND CHERNG-YUAN SUN****

**Department of Electronic Engineering*
National Lienho College of Technology and Commerce
Miaoli, Taiwan, R.O.C.
***Department of River and Harbor Engineering*
National Taiwan Ocean University
Keelung, Taiwan, R.O.C.
****Chung Shan Institute of Science and Technology*
Lungtan, Taoyuan, Taiwan, R.O.C.
*****Department of Electronic Engineering*
National Taiwan Institute of Technology
Taipei, Taiwan, R.O.C.

(Received May 17, 1994; Accepted November 15, 1995)

ABSTRACT

In X-ray lithography at deep submicron linewidths, the occurrence of thermal-induced dimensional instability of the mask structure under high-intensity X-ray irradiation is still a critical issue. To investigate the thermal effects of lithographic mask, a three-dimensional finite element technique in combination with a design-oriented methodology was used to simulate the distributions of temperature, stress, and displacement on an X-ray mask, which consisted of a thin silicon (Si) membrane carrying tungsten (W) absorber patterns. Some important results were derived from the present analysis: (1) the maximum temperatures occurred in the regions where the W absorber patterns were most densely populated; (2) the thermal stresses usually centered on the Si-W interface and the edges of W absorber; and (3) the thermoelastic displacements were directed from the center in the mask towards the mask edges. It was also shown that, for a mask structure with 0.25-μm minimum linewidth corresponding to the design rules of 256 Mb DRAM, the mask temperature variation must be maintained within 3.42 °C to suppress microdistortion to within the acceptable limit of 25 nm.

Key Words: X-ray lithography, thermal-induced dimensional instability, mask structure, finite element technique, silicon membrane, tungsten absorber, microdistortion.

I. Introduction

Considering the mass production of the next generation ULSI chips in the latter part of this decade, X-ray lithography (XRL) is now emerging as a very strong contender because of its clear potential for resolving features smaller than a tenth of a micron, and its significant processing advantages over coventional optical lithography, including its simple resist scheme, dust particle immunity, extreme depth of focus, and large field size (Hector *et al.*, 1993; Guo *et al.*, 1993). Especially from the viewpoint of cost, XRL is in a favorable position for the manufacture of high volume standard circuits such as dynamic random access memory (DRAM) chips due to its major assets of excellent process latitude, high throughput and yield (Koek *et al.*, 1993). Since the 256 Mb DRAM (0.25-μm design rule or minimum linewidth) is regarded as the first generation of ULSIs which cannot be produced economically by means of optical lithography, it will provide the first opportunity for bringing XRL into the semiconductor industry (Fleming *et al.*, 1992). In order to realize this opportunity, quarter-micron scale X-ray mask technology needs to be established first.

An X-ray mask consists of a membrane of low atomic weight material which has relatively good transparency for X-rays and a metallic absorbing pattern of high atomic weight material which has high X-ray stopping capability. The making of an X-ray mask is complicated by the fact that no thick, rigid, mask blank material which is transparent to soft X-rays is available. Therefore, very thin membrane (2~4μm thick) carrying X-ray opaque material (0.5~1μm thick) must be used, and there are problems of both durability and dimensional stability. Specifically, the mask may be subjected to substantial heating and thermal stress by high-

intensity X-ray sources during exposure, leading to a serious problem of mask distortion. If the magnitude of mask distortion exceeds 10% of the absorber minimum linewidth, the required mask-to-mask overlay accuracy for integrated circuit fabrication will deteriorate. Presently, both synchrotron storage rings and plasma sources are being extensively used as high power X-ray sources for lithography applications. Synchrotron radiation is generated when relativistic electrons in circular motion are deflected by a magnetic field, and it has nearly time-constant radiation power (Wilson, 1992). Since the synchrotron radiation reaching the mask is generally prefiltered by the grazing mirror and vacuum window inside the beamline (i.e., the radiation transport system), the maximum power on the mask is about 150 mW/cm^2. On the other hand, the plasma source is different in that radiation is emitted by a high temperature and density short-lived plasma, which is produced by either a high power laser source or an electrical discharge (Chaker *et al.*, 1992). The intensity is distributed isotropically and delivered in a very short time duration of 5~20 ns with extremely high power pulses amounting to 10^5~10^6 W/cm^2.

Because the fabrication and metrology of an X-ray mask are intricate, time consuming and very expensive, it is unreasonable to use a quantity of mask prototypes in conducting experiments to study thermal-induced mask distortions during the initial stage of mask design . Thus, an effective approach, like the finite element method, should be applied to probe the problems early in the design cycle to decrease costs and shorten the development time. Finite element models have been successfully used in many fields of engineering. Such models can in principle be made arbitrarily accurate by dividing the model into a sufficient number of elements. In this paper, the thermophysical response of an X-ray mask structure comprising a quarter-micron scale tungsten (W) absorber on silicon (Si) substrate membrane under high intensity X-ray irradiation was investigated by finite element modeling. In order to obtain reasonable numerical solutions, a design-oriented methodology was employed in the calculations. In other words, the models and assumptions adopted here were carefully planned in advance to approximate the practical configuration in XRL exposures. By using the commercially available MSC/NASTRAN finite element program with the IDEAS pre-post processor system, the transient behaviors of an X-ray mask regarding temperature, stress, and displacement were simulated. Also, a powerful CONVEX C210 minisupercomputer was used in the present work to deal with the extremely large amounts of data and to save computer time. The simulation results obtained in this study may be useful in defining future specifications for the design of 0.25-μm scale X-ray mask structures for 256 Mb DRAM.

II. Formulation

Incident X-ray power is transformed into heat energy by absorption in mask materials, primarily due to the photoelectric effect. The temperature rise of a mask subjected to intense soft X-rays irradiation depends on heat dissipating mechanisms with thermal conduction, radiation, and convection, and then on the mutual heat transfer among the membrane, absorber, surrounding gas, and wafer, as illustrated in Fig. 1. Consequently, the heat balance equation governing the temperature distribution in the mask can be expressed as follows (Chiba, 1992):

$$\frac{\partial T}{\partial t} = \frac{\phi}{\rho C}\left(\frac{\partial^2 T}{\partial x^2} - \frac{\psi}{\phi D}T\right) + \frac{H}{\rho C} - \frac{\eta\beta}{\rho C D}\left[(T+T_0)^4 - T_0^4\right], \tag{1}$$

where T is the temperature change (K), ϕ is the thermal conductivity, ρ is the density, C is the specific heat, ψ is the convective heat transfer coefficient, D is the thickness, H is the heat source due to absorption of X-rays, η is the emissivity, β is the Stefan-Boltzmann constant (=5.67 $\times$ 10^{-12}W cm^{-2}K^{-4}), and T_0 is the initial temperature.

As the influence of X-ray scattering is insignificant for soft X-ray lithography, Beer's law of absorption can be applied in the calculation of mask heating (Spiller, 1981). Assuming that the temperature variation along the film depth is uniform, the heat sources, H, can be written as follows:

$$H_m = \frac{I_0}{D_m}\left[1 - \exp(-\mu_m D_m)\right] \tag{2}$$

$$H_a = \frac{I_0}{D_a}\exp(-\mu_m D_m)\left[1 - \exp(-\mu_a D_a)\right] \tag{3}$$

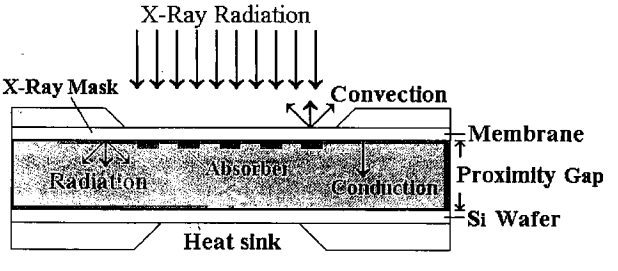

Fig. 1. Schematic diagram of the X-ray exposure setup and heat distribution mechanism.

$$H_p = \frac{I_0}{D_p} \exp(-\mu_m D_m - \mu_a D_a)[1 - \exp(-\mu_p D_p)], \quad (4)$$

where I_0 is the incident X-ray power density, and μ is the linear absorption coefficient. The subscripts m, a, and p represent the membrane, absorber, and proximity gap, respectively. The linear absorption coefficient at a wavelength of 10 Å is assumed.

Because the mask materials are extremely thin (only a few microns thick) when compared with the entire mask window size (normally several centimeters wide), the mask surface is considered to be in a state of plane stress; that is, the only nonzero stresses are σ_x, σ_y, τ_{xy}, and they are independent of the Z coordinate. Thus, the displacements, u and v, in the plane are also independent of Z. Assuming that the mask materials are linearly elastic isotropic, the thermal expansion coefficient α is the same for all directions. With Hooke's law for plane stress, we can relate the stresses to the strains, ε_x, ε_y and γ_{xy}, as described below:

$$\varepsilon_x = \frac{\partial u}{\partial x} = \frac{1}{E}(\sigma_x - \nu\sigma_y) + \alpha T(x, y, t) \quad (5)$$

$$\varepsilon_y = \frac{\partial v}{\partial y} = \frac{1}{E}(\sigma_y - \nu\sigma_x) + \alpha T(x, y, t) \quad (6)$$

$$\gamma_{xy} = \frac{\partial u}{\partial y} + \frac{\partial v}{\partial x} = \frac{2(1+\nu)}{E}\tau_{xy}. \quad (7)$$

In matrix form, the above equations become

$$\begin{Bmatrix} \sigma_x \\ \sigma_y \\ \tau_{xy} \end{Bmatrix} = \frac{E}{1-\nu^2}\begin{bmatrix} 1 & \nu & 0 \\ \nu & 1 & 0 \\ 0 & 0 & (1-\nu)/2 \end{bmatrix} \cdot \begin{Bmatrix} \varepsilon_x - \alpha T \\ \varepsilon_y - \alpha T \\ \gamma_{xy} \end{Bmatrix} \quad (8)$$

or

$$\{\sigma\} = [\Omega]\{\varepsilon - \varepsilon_0\}, \quad (9)$$

where ε_0 is the initial strain, E is the Young's modulus, ν is the Poisson's ratio, and $T(x, y, t)$ is the temperature profile on the mask surface. Based on the finite element formulation, a discretization form can be obtained.

III. Calculations

An X-ray mask structure with a 2-μm-thick Si membrane and a W absorber 0.8-μm thick was considered for computer simulations. The proposed layout of the Si-W mask structure is shown in Fig. 2. The Si membrane was a rectangle 6×7 μm, and the W absorbers (0.25-μm minimum linewidth) comprise typical geometric features normally encountered in a practical X-ray mask, such as a square pad, pillar, line and space gratings. The entire mask structure was assumed to be surrounded by a helium (He) environment. The values used in the calculations for the thermophysical parameters of the different materials are summarized in Table 1. In addition, two different X-ray sources were used in

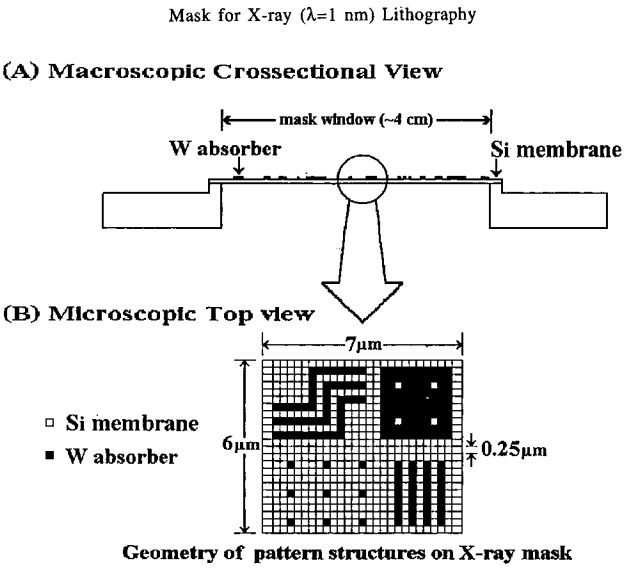

Fig. 2. Layout of the Si-W mask used in the calculations.

Table 1. Thermophysical Parameters Used in the Calculations

	Poisson ratio	Young's modulus $\times 10^{12}$ dyn/cm^2	Density g/cm^3	Thermal expansion 10^{-6}/°C	Thermal conductivity W/cm°C	Absorption coefficient μm^{-1}	Thickness μm	Specific heat J/kg°C
Si	0.28	1.30	2.30	2.33	1.57	0.203	2.0	712
W	0.40	3.45	19.3	4.50	1.78	5.003	0.8	132
He			1.8×10^{-4}		1.5×10^{-3}	5.39×10^{-7}	40	5193

the calculations. One was a synchrotron beam with a power density of 150 mW/cm^2, and the other was a plasma X-ray pulse with a power density of 5×10^5 W/cm^2 in a very short time duration of 10 ns. Table 2 shows the two cases considered, which were selected in order to simulate the actual operating conditions. The assumed X-ray wavelength was 10 Å.

The analysis of heat transfer in the mask structure (a solid continuum) can be reduced by finite element techniques to the solution of a set of equilibrium equations in which the unknowns are defined at a discrete set of points. Hence, the general equation that is solved when finite element methods are applied to heat transfer analysis may be written in the form (MS Corp., 1988)

$$[K]\{q\}+[B]\{\dot{q}\}=\{P\}+\{N\}, \qquad \textbf{(10)}$$

where $[K]$ is the symmetric matrix of the constant heat conduction coefficients, $\{q\}$ is the vector of the temperature at grid points, $[B]$ is the symmetric matrix of the constant heat capacity coefficients, $\{\dot{q}\}$ is the vector of the temperature gradient, $\{P\}$ is the vector of the applied heat flows that are known as a function of time, and $\{N\}$ is the vector of the nonlinear heat flows that depend on temperature. The detailed derivation can be found in the handbook of thermal analysis published by the MS Corporation (MS Corp., 1988). Heat transfer analysis with the MSC/NASTRAN program utilizes all of the normal analytical tools provided for structural analysis, the discrepancy being that the arrays $[K]$, $[B]$, $\{P\}$ and $\{N\}$ are computed from thermo-physical properties, rather than from structural properties.

For transient thermal analysis, the capabilities offered by MSC/NASTRAN Solution Sequence 89 (SOL 89) were used in the present study. After the temperature distribution was obtained, SOL 24 was employed in the stress analysis by assuming freedom from intrinsic stress. For the microscopic model construction, three layers of elements in the thickness direction were applied. Accordingly, the total number of solid elements and grids was 6480 and 7760, respectively. The finite element models used for the calculations are shown in Fig. 3.

Table 2. Computational Cases Considered

	Case 1	Case 2
Source type	Synchrotron radiation	Plasma pulse
Power density	150 mW/cm^2	5×10^8 mW/cm^2
Exposure time	1 sec	10 ns

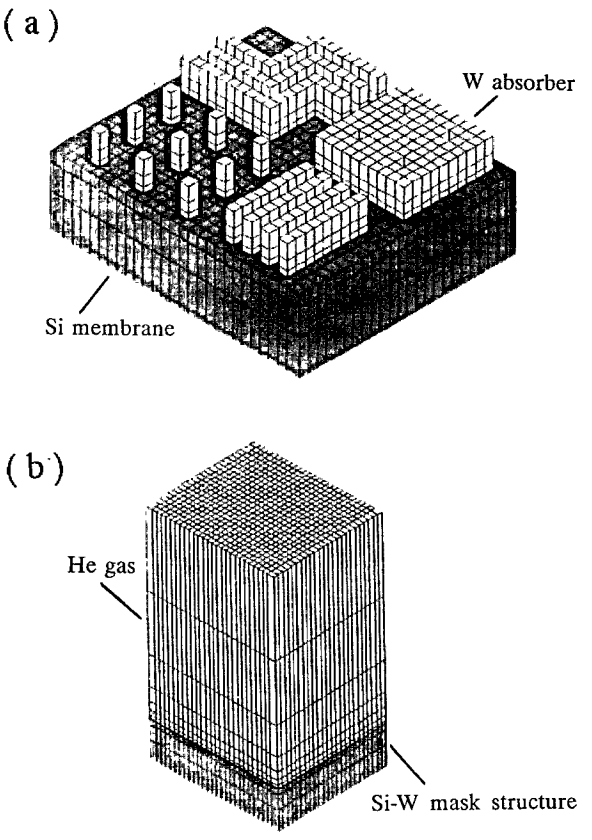

Fig. 3. Finite element models of the Si-W mask structure used in the calculations. (a) without He surrounding; (b) with He surrounding.

IV. Results and Discussions

When the mask was placed next to the wafer with a small proximity gap in an exposure chamber, the heat flowed from the irradiated mask surface into the He gas filling the gap and induced a free convection state. Due to an extremely small X-ray attenuation for He gas, the heat source due to absorption of X rays in the gap could be neglected. Since the static He gas boundary layer involved had an exceptionally large length magnitude (up to several centimeters) compared to the much smaller proximity distance (only 40 μm), the cooling effect resulting from free convection was negligible; therefore, thermal conduction from the mask through the surrounding He gas to the wafer (a heat sink with a constant temperature of 25°C) was the most important heat transfer mechanism.

1. Temperature and Thermal Stress Distributions

A. Case 1

Figure 4 illustrates the transient response of tem-

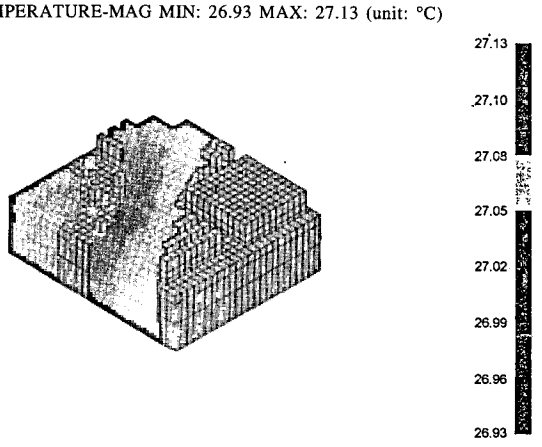

Fig. 4. Temperature distribution of the Si-W mask structure irradiated by a synchrotron source with 150 mW/cm^2 power density for a 1-sec exposure.

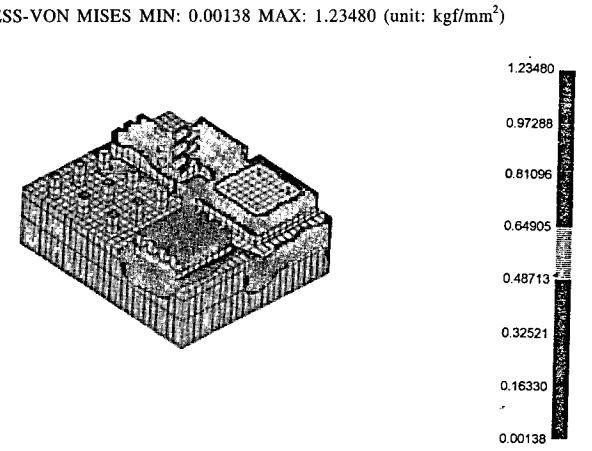

Fig. 5. Profile of the thermally-induced Von Mises's stress on the Si-W mask structure exposed by a synchrotron source with 150 mW/cm^2 power density for a 1-sec exposure. (1 kgf/mm^2=9.807 × 10^7 dyne/cm^2)

perature distribution on the mask structure for Case 1. Strip-like distinctive temperature zones are observed from this figure, indicating the existence of a temperature gradient from the region of the W square pad to the region of isolated pillars. It can be seen that higher peak temperatures occurred in the mask areas having a greater percentage of absorber coverage. This result is very reasonable in view of the fact that more than 98% of the incoming X-ray power was absorbed by the mask regions covered by the W pattern; i.e., almost all of the X-ray flux incident on the W absorber was absorbed whereas the uncovered regions absorbed only about 2%. As shown in Fig. 4, the maximum temperature (27.13°C) took place in the region of the W square pad where the density of absorber coverage was highest, and the heat was transferred in a diagonal direction from right to left.

The results of thermal stress calculations for the mask structure are shown in Fig. 5. It is observed that the thermal-induced stresses were concentrated on the Si-W interface of the square pad and gratings. The calculated maximum Von Mises's stress (i.e., square root of the sum of the the squares of all stresses) at the Si-W interface was 1.2×10^8 dyn/cm^2. The mismatch of thermal expansion coefficients between the W absorber and Si substrate could be expected to contribute to the buildup of thermal stress at the interface region. Therefore, in this case and under the worst condition, the most probable means of mask failure is peeling of the W absorber from the Si membrane as a consequence of induced shear stress at the interface which exceeds the adhesion strength between them.

Currently, X-ray mask design sometimes uses an intermediate layer (e.g., chromium, lead, or platinum) to provide adequate bonding between the mask absorber and membrane. Because such intermediate layers are very thin (200~300 Å), any defect in the layers may initiate cracks and subsequent stress cumulation at the interface regions, leading to fatal denudation of the absorber from the membrane. Therefore, application of such interface materials as adhesion promoters must be done very carefuly in mask design.

B. Case 2

A plot of the temperature distribution on the mask structure irradiated by a 10-ns X-ray pulse is shown in Fig. 6. It is observed that the maximum temperature of 28.25°C occurred at the W square pad, where the heat was transferred through the thickness of the W absorber. Figure 7 illustrates the time dependence of the calculated temperature at the points on the upper layer and bottom layer of the W absorber. The temperature of the point on the upper layer reached a maximum at the end of the pulse (i.e., 10 ns) and then exponentially decayed to a uniform temperature on a timescale of order 25 ns due to the heat conduction through the W absorber into the Si membrane. On the other hand, the temperature of the point on the bottom layer of the W absorber (near the Si-W interface) showed essentially an increase during the length of the pulse, and then it stabilized at the same temperature of the point on the upper layer of the W absorber, representing that the thermal equilibrium state was eventually

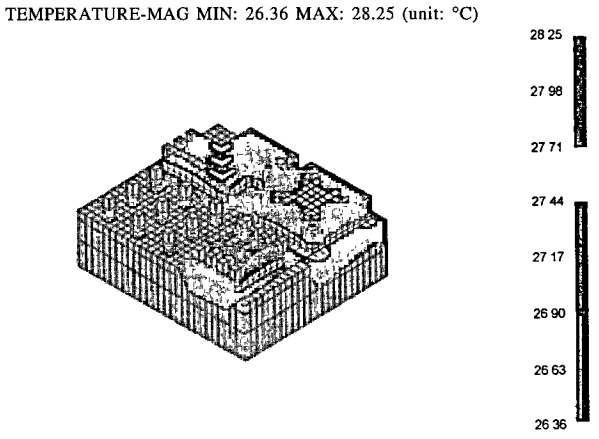

Fig. 6. Temperature distribution of the Si-W mask structure after a 10-ns, 5×10^8 mW/cm^2 plasma X-ray pulse.

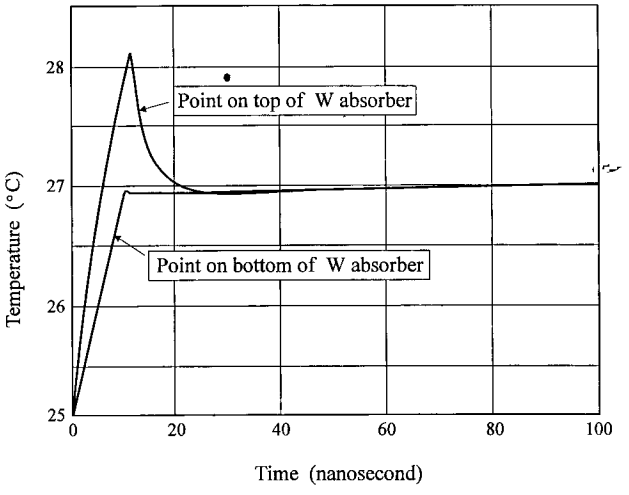

Fig. 7. Time dependence of the calculated temperature on the W absorber due to a 10-ns plasma X-ray pulse.

reached.

Since the duration of the high-intensity pulsed X-ray irradiation was very short, especially compared to the estimated time needed for heat propagation from the mask through the helium gas to the cooled wafer (several microseconds), serious thermal impact problems could arise with the plasma source. The stress calculations of the mask structure for Case 2 shown in Fig. 8 indicate that the thermal stresses not only centered on the Si-W interface, but also on the region around vias on the W square pad. The maximum calculated stress value in Case 2 was 1.6×10^8 dyn/cm^2, which was somewhat higher than that in the Case

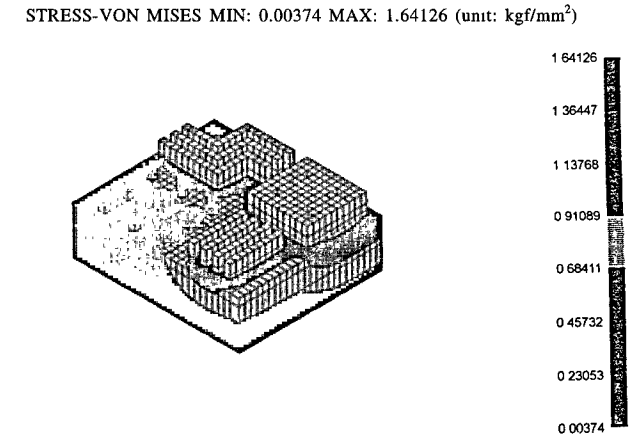

Fig. 8. Profile of the thermally-induced Von Mises's stress on the Si-W mask structure after a 10-ns, 5×10^8 W/cm^2 plasma X-ray pulse. (1 kgf/mm^2=9.807×10^7 dyne/cm^2)

1. It is also observed from the figure that large stress could be induced in the vicinity of the edges (i.e., the corner points) of the W absorbers. The corner points were the locations where mask failure could take place in either the form of excess plastic strain or in the mode of absorber delamination resulting from shear loading. It is therefore reasonable to doubt that thermal cycling generated by repetitive X-ray pulses can result in unwanted mask distortion and lifetime problems. Based on the simulated results, it is suggested that there is a need to conduct acceleration testing for thermal stress-induced mask failure to evaluate the mask thermal stability and failure threshold.

2. Pattern Displacement Contour

The calculations of temperature distributions presented above show that mask temperature rises were kept under 3.3°C by using He gas to thermally connect the mask to the wafer (i.e., mask-wafer thermal coupling). Even though the temperature was low, the thermal distortion problem could occur when the temperature gradient existed. The effect of such small temperature rises on nonlinear absorber pattern stability and overlay accuracy involved in the lithography process is still an open question.

An important and identical result obtained from the displacement analysis of the mask structure for both the synchrotron and plasma source, as shown in Fig. 9, indicates that thermoelastic displacements were directed from the center in the mask towards the mask edges. This result suggests that during X-ray exposure

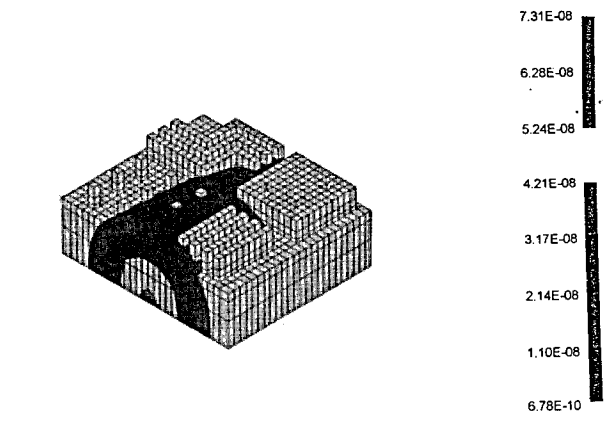

Fig. 9. Graphic plot of the thermal displacement on the Si-W mask structure after X-ray irradiation.

the in-plane distortions on the mask were not fixed but shifted outward; that is, the behavior of thermal distortions was dynamic response. In this case, the mask was expanding. It is considered that the direction of shift resulted from the thermal stresses acting toward the mask rims. We therefore presume that the feature edges of the printed image on the wafer would blur due to the in-plane motion of points on the mask. This prediction is in good agreement with similar experimental results observed by a number of previous researchers (Vladimirsky *et al.*, 1989).

This thermal-induced pattern displacement, caused by the local temperature change during the lithography process, was determined by the X-ray power absorbed in the mask, the heat loss mechanism, and the elastic and geometric properties of the mask material. An estimate of the maximum displacement for the Si-W mask structure predicts a magnitude of $\delta_{max}=7.31 \times 10^{-8}\Delta T$ mm. In general, the absorber feature position shift must be restricted to within one tenth of the minimum feature size (critical dimension). For the quarter-micron design rule of 256 Mb DRAM, the value of δ_{max} should be within 0.025 μm. This means that the temperature change needs to be controlled to within 3.42°C (initial temperature: 25°C). In other words, the tolerable maximum and minimum temperatures are 28.42°C and 21.58°C, respectively. This interpretation of the temperature control in the mask/wafer unit is an important issue which must be taken into account to avoid unexpected temperature variation arising under certain conditions, such as cooling system breakdown or poor cooling design.

V. Conclusions

The influence of heavy X-ray irradiation on the thermophysical behavior of a silicon-tungsten (Si-W) mask structure in semiconductor microlithography was examined by numerical simulation. To approach realistic physical conditions in X-ray lithographic exposure, a relatively large three-dimensional finite element model with 6480 elements and 7760 grids was created to simulate the Si-W mask under thermal loading. The finite element calculation was carried out by using the commercially available MSC/NASTRAN program with the IDEAS pre-post processor system on a powerful CONVEX C210 minisupercomputer. Investigations focused on the temperature distrubutions, the thermal stress profiles, and the thermal displacement contour in the Si-W mask structure. The simulated results can provide both qualitative and quantitative information for optimal mask-design to minimize in-plane thermal distortion, as follows:

(1) A more densely populated absorber pattern is expected to produce higher peak temperatures. The maximum temperature is found to take place at the W square pad, which locally has greatest percentage coverage on the Si mask membrane.

(2) The thermally-induced stresses are prone to accumulate at the Si-W interface and the corners of W feature. Furthermore, in the case of a plasma source, it is of interest that the thermal stresses also build up in the vicinity of voids on the W square pad.

(3) During X-ray exposure, the temperature-induced pattern position shift or in-plane thermal distortions are directed outward. This phenomenon indicates that the thermal stresses in the W absorber and the Si membrane act toward the edges of the mask structure.

(4) In order to keep the thermoelastic displacement below 0.025 μm for the Si-W mask designed with a critical dimension of 0.25 μm, precise control of localized temperature variation to within 3.42°C is needed.

(5) Under the conditions assumed in this study, it is confirmed that the temperature rises, and that corresponding thermoelastic distortions on the mask can be accommodated within acceptable limits when using helium, which has a high thermal conductivity and absorbs little X-ray flux, as a heat exchange medium.

Acknowledgments

The authors wish to thank the National Science Council, ROC, for financial support of this work.

References

Chaker, M., B. L. Fontaine, C. Y. Cote, J. C. Kieffer, and H. Pepin (1992) Laser plasma sources for proximity printing x-ray lithography. *J. Vac. Sci. Technol.*, **B10**, 3239-3244.

Chiba, A. (1992) Dynamic in-plane motion of an x-ray mask membrane induced by synchrotron radiation irradiation. *Jpn. J. Appl. Phys.*, **31**, 2949-2955.

Fleming, D., J. R. Maldonado, and M. Neisser (1992) Prospects for x-ray lithography. *J. Vac. Sci. Technol.*, **B10**, 2511-2515.

Guo, Z. Y., Q. Leonard, F. Cerrina, E. D. Fabrizio, L. Luciani, M. Gentili, and J. Frank (1993) Experimental study of aerial images in x-ray lithography. *J. Vac. Sci. Technol.*, **B11**, 2902-2905.

Hector, S. D., H. I. Smith, and M. L. Schattenburg (1993) Simultaneous optimization of spectrum, spatial coherence, gap, feature bias, and absorber thickness in synchrotron-based x-ray lithography. *J. Vac. Sci. Technol.*, **B11**, 2981-2985.

Koek, B., B. Jennings, and R. Grant (1993) Patterning issues of 256 Mb dynamic random access memory x-ray masks. *J. Vac. Sci. Technol.*, **B11**, 2876-2880.

Macneal-Schwendler Corp. (1988) *Handbook for Thermal Analysis,* MSC/NASTRAN Version 65.

Munchmeyer, D. and J. Langen (1992) Manufacture of three-dimensional microdevices using synchrotron radiation. *Rev. Sci. Instrum.*, **63**, 713-718.

Spiller, E. (1981) High resolution soft x-ray optics. *Proc. SPIE*, **95**, 316-322.

Vladimirsky, Y., J. Maldonado, R. Fair, R. Acosta, R. Viswanathan, R. Voelker, F. Cerrina, and R. Nachman (1989) Thermal effects in x-ray masks during synchrotron storage ring irradiation. *J. Vac. Sci. Technol.*, **B7**, 1657-1662.

Wilson, M. N. (1992) Superconducting compact sources for lithography. *Rev. Sci. Instrum.*, **63**, 707-713.

0.25微米X光成像光罩之熱物理計算

李子琦* 陳正宗** 全湘偉*** 孫澄源****

*聯合工商專校電子工程科

**海洋大學河海工程系

***中山科學研究院

****工業技術學院電子工程技術系

摘 要

對於用以解析深次微米線寬之X光成像術而言，其光罩結構在承受高強度X光輻射時所引發之熱不穩定性，仍爲一關鍵性課題。爲了探討X光光罩在曝光時之熱效應，本文應用三維固體元有限元素分析技術配合設計導向方法來模擬矽—鎢光罩結構之瞬間溫度變化、熱應力與位移分佈。根據計算結果得知：(1)最大溫度值發生在鎢膜構體分佈密度最高之區域；(2)熱應力通常集中在矽—鎢介面與鎢膜構體轉角處；(3)熱彈性位移往光罩外徑邊緣移動。而針對256 Mb動態隨機記憶體所需之0.25微米設計規範之X光光罩來說，光罩之溫度變化必須維持在3.42℃之範圍內，以控制其熱彈性變形量在25nm之容許值以內。